Global Environmental Science
www.sciltp.com/journals/ges

Article

The Effect of Aniline Pretreatment on Pt/CeO_2 Nanocatalysts for Boosting Toluene Oxidation

Dengfeng Yan [1,*,†], Zhentao Feng [2,†], Yuhao Wang [3], Xudong Li [1], Siyuan Gao [1] and Daiqi Ye [4,*]

[1] Guangdong Research Center of Occupational Hygiene, Guangdong Province Hospital for Occupational Disease Prevention and Treatment (GDHOD), Guangzhou 510399, China
[2] Dongguan Environmental Protection Industry Promotion Center, Dongguan 523000, China
[3] Guangzhou Center for Disease Control and Prevention (Guangzhou Health Supervision Institute), Guangzhou 510440, China
[4] School of Environment and Energy, South China University of Technology, Guangzhou 510006, China
* Correspondence: 745279897@qq.com (D.Y.); cedqye@scut.edu.cn (D.Y.)
† These authors contributed equally to this work.

How To Cite: Yan, D.; Feng, Z.; Wang, Y.; et al. The Effect of Aniline Pretreatment on Pt/CeO_2 Nanocatalysts for Boosting Toluene Oxidation. *Glob. Environ. Sci.* **2025**, *1*(1), 69–78. https://doi.org/10.53941/ges.2025.100007

Publication History

Received: 28 May 2025
Revised: 8 July 2025
Accepted: 29 July 2025
Published: 7 August 2025

Keywords

volatile organic compounds; Pt/CeO_2; metal-support interaction; catalytic combustion; aniline pretreatment

Abstract: A comprehensive study was conducted to explore an innovative strategy aimed at enhancing the catalytic activity and longevity of Pt-supported CeO_2 nanocatalysts through the pretreatment with aniline. The introduction of aniline was found to effectively induce and strengthen the strong metal-support interaction (SMSI) within the Pt-supported CeO_2 nanocatalysts, yielding a substantial increase in catalytic performance. Specifically, the T_{90} value for the 0.9Pt/CeO_2-A catalyst was determined to be 149 °C when subjected to a toluene concentration of 1000 ppm in a dry air mixture at a weight hourly space velocity of 48,000 mL g^{-1} h^{-1}. Extensive experimental analyses conducted using techniques such as X-ray photoelectron spectroscopy (XPS), transmission electron microscopy (TEM), and visible Raman spectroscopy revealed that the modification via aniline significantly alters the physicochemical properties of the Pt/CeO_2 system. Notable changes included an increase in the concentration of Pt^0 and Ce^{3+} ions, a reduction in Pt particle size, and a corresponding increase in surface oxygen vacancies. These modifications are posited to be pivotal in the enhancement of both catalytic activity and durability. The findings of this investigation suggest that the methodological approach delineated herein may represent a universal strategy for augmenting the activity and stability of other noble metal-supported CeO_2 nanocatalysts.

Highlights

- The aniline was effectively utilized to modify various Pt/CeO_2 catalysts
- Aniline pretreatment strengthens the SMSI in Pt/CeO_2 catalyst
- The 0.9Pt/CeO_2-A catalyst exhibits excellent activity and stability for toluene catalytic oxidation

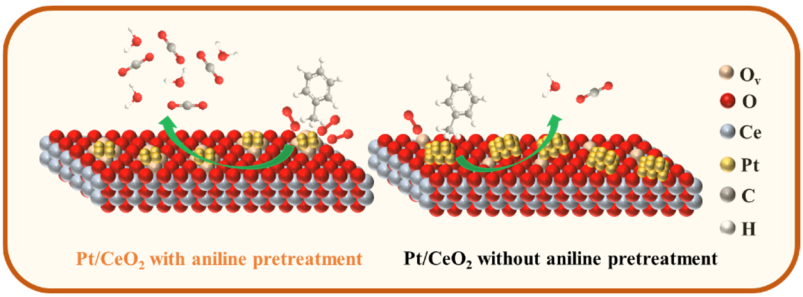

1. Introduction

The mitigation of volatile organic compounds (VOCs) emissions from chemical manufacturing facilities and vehicular sources represents a pivotal area of focus for effectively addressing urban air quality degradation [1,2]. These compounds are associated with considerable risks to public health and environmental integrity, attributable to their toxic, mutagenic, carcinogenic, and teratogenic characteristics [3,4]. Over the past several decades, substantial advancements have been realized in the

development of technologies aimed at controlling VOC emissions. Among these, catalytic oxidation has emerged as a particularly promising technique, demonstrating significant efficacy in pollutant removal, economic feasibility, and the generation of minimal organic by-products [5,6]. Recent innovations in catalytic materials, including noble metal-supported (NMs) catalysts [7] and transition-metal oxide catalysts [8], indicate considerable potential for further enhancements in catalytic efficacy.

The use of NMs catalysts, especially Pt-based materials [9–11], has long been a subject of great interest in catalytic combustion. These catalysts exhibit unique catalytic properties that set them apart from conventional noble metals and transition metal oxides. This distinctiveness is largely due to the strong interaction between Pt nanoclusters and the oxide support [12–14]. The interaction between Pt and the oxide support is of particular importance, as it influences not only the formation of oxygen vacancies but also the morphology of Pt nanoparticles. Additionally, this interaction affects the chemical states of both metal and Pt ions, as well as the charge transfer dynamics at the interfacial sites. Collectively, these factors significantly contribute to the catalytic efficacy of Pt-based catalysts [9,15–18]. Consequently, achieving a profound understanding of and optimizing the strong metal-support interaction (SMSI) at the metal/oxide interface emerges as a critical factor in the advancement of high-performance catalytic systems [19–21].

The SMSI can significantly influence catalytic activity, either enhancing or hindering it. Therefore, it is imperative to develop effective methods to control or adjust the SMSI effect, ensuring improved catalytic performance without sacrificing activity. Ge et al. introduced a novel strategy aimed at augmenting the metal-support interaction of the Pt/CeO_2 catalyst through the careful adjustment of Pt nanoparticle size. Their findings indicate that Pt nanoparticles with diameters smaller than 4 nm tend to transfer electrons to the CeO_2 support, a phenomenon that proves detrimental to the activation of propane adsorption, ultimately leading to a decline in propane oxidation performance [18]. In a complementary approach, Zhang et al. methodically adjusted the activation conditions to finely tune the Metal-Support Interaction (MSI). Their research revealed that a weakened MSI resulted in an increase in the electron density of Pt, thereby enhancing the activation of oxygen adsorption while simultaneously mitigating CO poisoning; however, it also hindered CO adsorption activation on platinum [15]. The effect of SMSI on the oxidative performance of catalysts was precisely characterized as a double-edged sword by Peng et al. [10]. This requires us to regulate SMSI more precisely for Pt/CeO_2 catalyst to maximize its oxidation performance on toluene.

Recent studies have demonstrated that nitrogen atoms present in aniline effectively bind to platinum ions (such as Pt^{2+} or Pt^{4+}) through coordination bonds, resulting in the formation of a stable Pt-N coordination complex. The benzene ring groups on the aniline stack on the support surface, further creating a restricted spatial environment for the Pt ions. These two factors contribute significantly to the high dispersion of Pt nanoparticles on the support surface [22]. A sacrificial carbon layer is strategically constructed on the surface of Pt nanoparticles through the calcination of Pt^{2+}/aniline/CeO_2 complexes in an inert atmosphere. This layer serves as a "protective shell," effectively preventing the aggregation and growth of precious metal particles at elevated temperatures while preserving their high degree of dispersion. The subsequent oxidative calcination in air facilitates the removal of the carbon layer, a process characterized by the loss of electrons. This removal enhances the contact between the metal and the support and intensifies electronic interactions, thereby improving the thermal stability of the catalyst [23]. Following the elimination of the carbon layer, nitrogen atoms can be doped into the support oxides, which leads to the generation of numerous oxygen vacancies. This modification provides additional sites for the activation of oxygen, resulting in a significant enhancement of the catalytic activity in oxidation reactions [24].

In this investigation, we implemented a modification technique involving an aniline-dispersed sacrificial carbon layer, referred to as aniline pretreatment, to enhance the performance of catalysts. A comprehensive comparative analysis was conducted to evaluate the catalytic efficiency of the Pt/CeO_2 catalysts before and after modification. Noteworthy findings indicate a significant enhancement in the catalytic activity of the modified Pt/CeO_2 catalysts in the degradation of toluene, a phenomenon that appeared to be consistent regardless of the loading content. The physicochemical properties of the catalysts, both pre-and post-modification, were meticulously characterized using transmission electron microscopy (TEM), X-ray photoelectron spectroscopy (XPS), and Raman spectroscopy. Additionally, we initiated an in-depth investigation into the underlying mechanisms associated with the modification process.

2. Results and Discussion

2.1. Characterization of Physicochemical Properties of Catalysts

The morphology of CeO_2 and Pt supported samples was meticulously analyzed using TEM and high-resolution transmission electron microscopy (HRTEM), as depicted in Figure 1. In panels (a–d) of Figure 1, the CeO_2 support is characterized by well-defined cubic morphologies, exhibiting a d-spacing of 0.27 nm, which corresponds to the (200) crystal plane of CeO_2. The selected area electron diffraction (SAED) pattern further corroborates the single-crystal structure of the CeO_2

 https://doi.org/10.53941/ges.2025.100007

sample. Conversely, in panels (e–l), it is evident that the CeO_2 support retains its cubic morphology post-Pt loading, demonstrating d-spacing values of 0.19 nm and 0.27 nm, which can be ascribed to the (100) crystal plane of Pt and the (200) crystal plane of CeO_2, respectively. The resulting SAED pattern suggests the presence of a mixed-crystal structure for the CeO_2 support following Pt incorporation. Furthermore, the average sizes of Pt nanoparticles were ascertained by evaluating around 100 Pt nanoparticles from HRTEM images. It is noteworthy that the size of Pt on the 0.9Pt/CeO_2-A sample (2.4 nm) was found to be smaller than that of the 0.9Pt/CeO_2 sample (3.1 nm), thereby indicating an enhancement in Pt dispersion subsequent to aniline pretreatment. Additionally, a conformal crystalline bilayer coating was observed on larger crystalline Pt particles, as highlighted by the red line in Figure 1, which may be attributed to the CeO_x formation induced by the strong metal-support interaction (SMSI) [25].

The XRD patterns of all the samples with varying Pt loadings are illustrated in Figure 2. A comparative analysis with the standard CeO_2 diffraction card reveals that all samples exhibit a characteristic crystalline fluorite structure, corresponding to the space group Fm-3m [26]. Notably, no diffraction peaks corresponding to Pt or PtO_x species are observed in Figure 2, indicating that Pt is well dispersed on the CeO_2 surface. The mean crystallite sizes calculated via the Scherrer equation indicate minimal variation following Pt loading, as summarized in Table 1. Furthermore, the lattice parameters of the catalysts, as indicated in Table 1, demonstrate a decrease upon the incorporation of Pt. This decrease may be attributed to the partial entry of Pt^{2+} (r = 0.074 nm) or Pt^{4+} (r = 0.076 nm) into the fluorite-like lattice CeO_2 (r = 0.094 nm), leading to the formation of a Pt-O-Ce solid solution and resulting in the shrinkage of the unit cell [27].

The analysis of the Pt loading content, dispersion, and specific surface area of the catalysts was conducted using ICP-AAS, static CO chemisorption, and N_2 adsorption and desorption isotherms, respectively. The results, as presented in Table 1, reveal that the attained Pt concentrations closely match the expected values for each sample, indicating the highly efficient deposition of Pt on the CeO_2 surface. The BET specific surface areas of the samples remained almost unchanged after Pt loading, with values of 62.7, 59.6, 60.4, 60.9 and 59.7 $m^2\ g^{-1}$, respectively. It is worth noting that the Pt dispersion of 0.6Pt/CeO_2-A and 0.9Pt/CeO_2-A was observed to be higher than that of 0.6Pt/CeO_2 and 0.6Pt/CeO_2, likely attributable to the strong metal-support interaction (SMSI) between Pt particles and CeO_2 support, effectively hindering the sintering of small Pt nanoparticles [23]. In the process of preparing the Pt/CeO_2-A catalyst, aniline plays a crucial role as an amphiphilic molecule, effectively serving as a surface-active agent in the dispersion of Pt^{4+}. The benzene ring in aniline is adsorbed onto the defect sites of the CeO_2 surface, while the amino group, functioning as the hydrophilic group, is oriented towards the solvent phase. Consequently, aniline serves a dual role as a dispersant and a stabilizer of Pt^{4+}, as illustrated in Scheme 1. It facilitate the uniform dispersion of Pt particles throughout the carbonization process and contributes to the formation of a protective carbon layer. This layer is significant as it mitigates the agglomeration of Pt particles during subsequent high-temperature oxidation, thereby ensuring the maintenance of a highly dispersed state of platinum particles in aniline-modified catalysts.

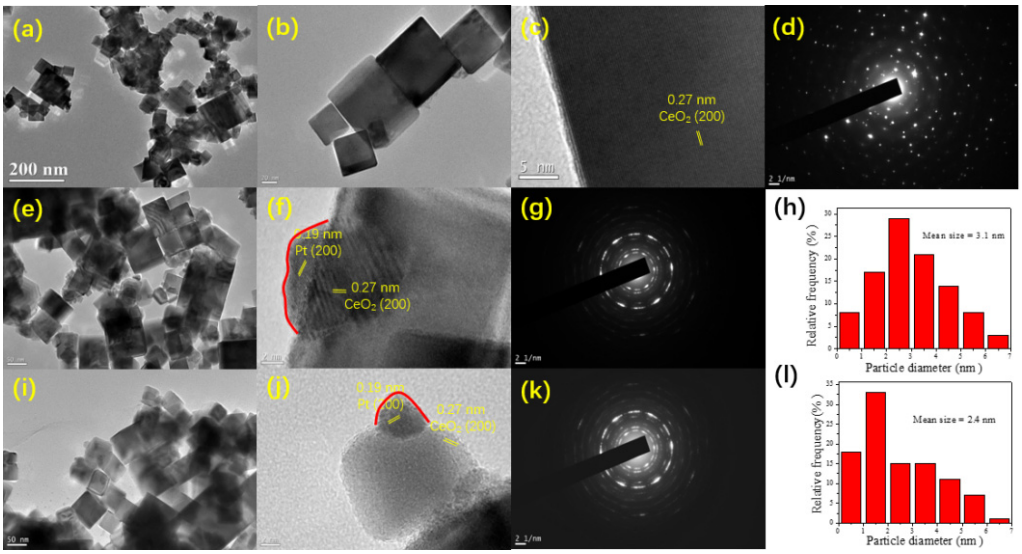

Figure 1. TEM, HRTEM, selected area electron diffraction (SAED) and size distribution images of the samples: (**a**–**d**) CeO_2; (**e**–**h**) 0.9Pt/CeO_2; (**i**–**l**) 0.9Pt/CeO_2-A.

The chemical composition of Ce species, O species, Pt species, and N species on the catalyst's surface is determined using XPS measurements. The Ce 3d spectra display ten peaks resulting from a double-precision pair of

rotating orbits, as outlined in the literature (as depicted in Figure 3a) [28]. The peaks of V^0 (880.6 eV), U^0 (898.6 eV), V′ (883.9 eV), and U′ (901.9 eV) are indicative of Ce^{3+}, suggesting the presence of oxygen vacancies on the CeO_2 surface. Conversely, the peaks of U (900.3 eV), U″ (906.9 eV), U‴ (916.1 eV), V (881.9 eV), V″ (888.5 eV) and V‴ (897.6 eV) can be attributed to Ce^{4+}. The proportions of trivalent CeO_2 are detailed in Table 2. Notably, catalysts modified by aniline exhibit relatively higher Ce^{3+} contents, indicating the presence of more oxygen vacancies and potentially higher reaction activity. In the Pt/CeO_2 catalysts, the O 1s displays two separate peaks, which can be attributed to O_{sur} and O_{latt} (as illustrated in Figure 3b and detailed in Table 2). The increased presence of O_{sur} may be linked to a higher concentration of vacancies, a finding consistent with the Ce^{3+} results.

As illustrated in Figure 3c, the Pt 4f spectrum comprises four discernible peaks: 72.6 eV and 73.7 eV for Pt $4f_{7/2}$, and 75.8 eV and 77.2 eV for Pt $4f_{5/2}$. It is noted in the literature that the peaks at 72.6 eV and 75.8 eV correspond to zero-valent platinum species, while the peaks at 73.7 eV and 77.2 eV are indicative of bivalent platinum species. The Pt^0 content was determined by calculating the composition of different Pt species ($Pt^0/(Pt^0 + Pt^{2+})$), as presented in Table 2, and exhibited minimal variation across all samples. However, the Pt^{2+} peaks of $0.6Pt/CeO_2$-A and $0.9Pt/CeO_2$-A (around 74.6 eV) have shifted to a higher binding energy compared to that of $0.6Pt/CeO_2$ and $0.6Pt/CeO_2$ (around 74.3 eV), attributed to the enhanced strong metal-support interaction after aniline pretreatment [29].

The N 1s XPS spectra of $0.6Pt/CeO_2$-A and $0.6Pt/CeO_2$-A were analyzed and compared to elucidate the potential influence of N on Pt-Ce interaction. The profiles are shown in Figure 3d. The spectra exhibit three main peaks at 398.1 eV (N1), 399.5 eV (N2), and 402.1 eV (N3), corresponding to the pyridine-like (or perhaps the Pt–N compound), pyrrole-like nitrogen, and the surface NO_x species, respectively [30]. The ratio of N1/(N1 + N2 + N3) serves as an indirect indicator of the nitrogen species' presence on the catalyst surface, thereby influencing the interaction between Pt and Ce. Analysis of Table 2 indicates that $0.9Pt/CeO_2$-A has a higher N1/(N1 + N2 + N3) than $0.6Pt/CeO_2$-A, suggesting a stronger SMSI in $0.9Pt/CeO_2$-A. Additionally, the presence of N also influences the state of charge of surrounding atoms, potentially accounting for the position shift of the Pt^{2+} peak in Figure 3c. Notably, the Pt-N bond, characterized by its shorter length and comparatively high bond energy, presents greater resistance to migration and aggregation of Pt on the support surface when contrasted with the Pt-O bond. This attribute contributes to the enhanced thermal stability of the catalyst [31].

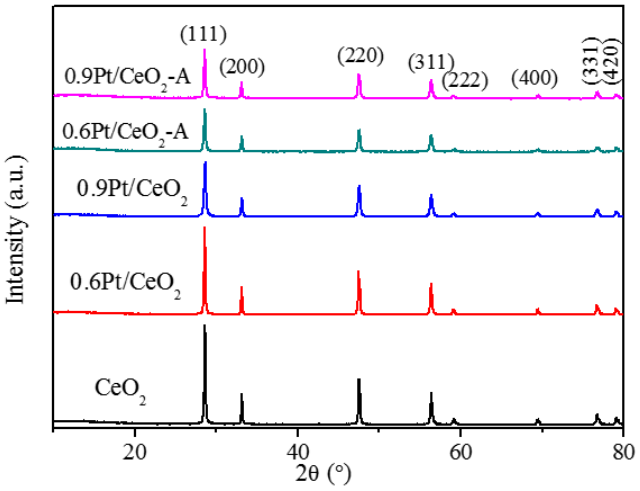

Figure 2. XRD patterns of CeO_2, $0.6Pt/CeO_2$, $0.9Pt/CeO_2$, $0.6Pt/CeO_2$-A and $0.9Pt/CeO_2$-A catalysts.

Oxygen vacancies on ceria serve as active sites that significantly influence catalytic activities in relevant applications. Figure 4a illustrates the UV Raman spectra of various samples, as detailed in Table 2. The prominent peaks observed at 458 cm^{-1}, 592 cm^{-1} and 1180 cm^{-1}. These peaks are indicative of key vibrational modes: the symmetric stretching vibration of O^{2-} around Ce^{4+}(F_{2g}) within the cubic fluorite framework of ceria, defect-induced band (D) patterns associated with oxygen vacancies and second-order longitudinal optical (2LO) modes related to presence of Ce^{3+}, respectively [27]. The concentration of oxygen vacancies can be effectively evaluated through the ratio of I_D and I_{F2g}. The findings indicate a ranking of $0.9Pt/CeO_2$-A > $0.9Pt/CeO_2$ > $0.6Pt/CeO_2$-A > $0.6Pt/CeO_2$ > CeO_2, suggesting that both Pt loading and aniline pretreatment facilitate the formation of oxygen vacancies. indicates that Pt loading and aniline pretreatment are beneficial for the oxygen vacancies formation. Based on the XPS data, it is postulated that the observed phenomena may be attributed to the transfer of electrons from carbon oxidation during the sacrificial carbon layer process. This electron transfer appears to facilitate the reduction of a portion of Ce^{4+} to Ce^{3+}. Concurrently, part of N atoms doped onto CeO_2 support likely contributes to the generation of defects, resulting in an increased abundance of oxygen vacancies on the catalyst. This enhancement in oxygen vacancy concentration may subsequently lead to improved catalytic performance. To further elucidate the SMSI between Pt and CeO_2, we employed visible Raman spectroscopy, with the results presented in Figure 4b. Previous studies have indicated that the Raman peaks observed at ~565 cm^{-1} and ~700 cm^{-1} correspond to the vibrations of Pt-O-Ce bridge vibration and the Pt-O bond within the Pt-O-Ce complex, respectively [27]. The detailed analysis presented in Figure 4b substantiates that when Pt is deposited onto CeO_2, the Pt atoms are anchored to the surface oxygen of CeO_2, leading to the

 https://doi.org/10.53941/ges.2025.100007

formation of the Pt-O-Ce bond. This phenomenon arises from the strong metal-support interactions between Pt nanoparticles and the CeO_2 support [32]. Furthermore, it is important to highlight that the strength of the Pt-O-Ce bond is markedly improved in samples that have undergone aniline pretreatment. This enhancement is hypothesized to result from the substantial electron transfer associated with carbon oxidation during the sacrificial carbon layer process. Such phenomena likely augment the electronic interactions between Pt and CeO_2, thereby reinforcing the metal-support interface. Our Pervious research by supports the notion that a stronger Pt-O-Ce bond is advantageous as it prevents the agglomeration of Pt, thus maintaining its superior dispersion on the CeO_2 support [32]. Consequently, the Pt/CeO_2-A samples are anticipated to exhibit superior durability compared to the Pt/CeO_2 samples lacking aniline modification.

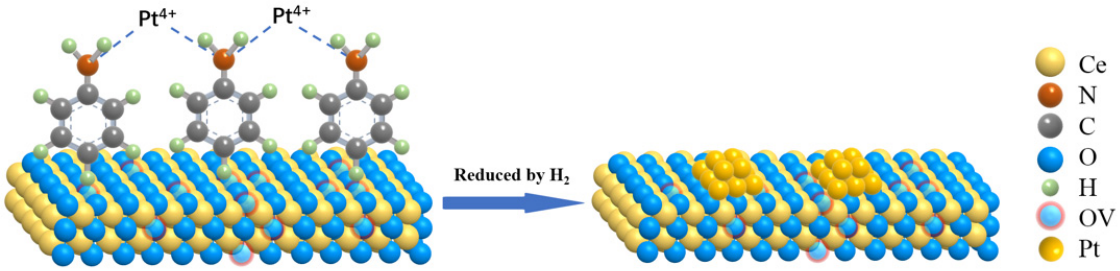

Scheme 1. Schematic illustration of aniline promotes Pt dispersion and stability.

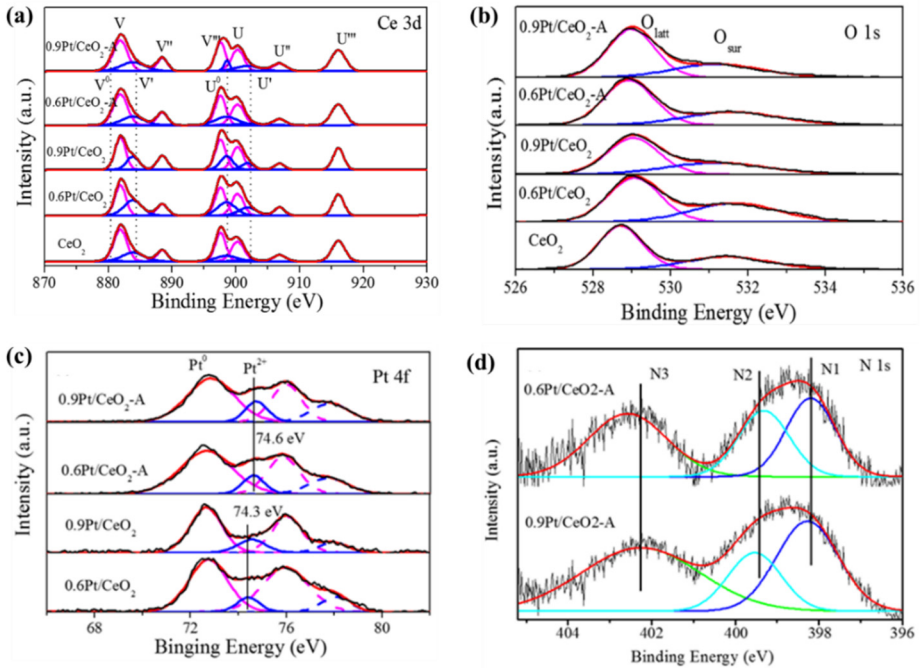

Figure 3. XPS spectra of (**a**) Ce 3d, (**b**) O 1s, (**c**) Pt 4f and (**d**) N 1s for CeO_2, $0.6Pt/CeO_2$, $0.9Pt/CeO_2$, $0.6Pt/CeO_2$-A and $0.9Pt/CeO_2$-A catalysts.

Table 1. Structural properties of CeO_2, $0.6Pt/CeO_2$, $0.9Pt/CeO_2$, $0.6Pt/CeO_2$-A and $0.9Pt/CeO_2$-A catalysts.

Samples	Pt Loading [a] (wt.%)	Pt Dispersion [b] (%)	S_{BET} [c] ($m^2\ g^{-1}$)	Mean Size [d] (nm)	Lattice Parameter [e] (nm)
CeO_2	/	/	62.7	50.3	0.54128
$0.6Pt/CeO_2$	0.59	72.9	59.6	51.3	0.54123
$0.9Pt/CeO_2$	0.88	63.5	60.4	51.1	0.54117
$0.6Pt/CeO_2$-A	0.59	79.7	60.9	50.6	0.54121
$0.9Pt/CeO_2$-A	0.89	74.2	59.7	50.9	0.54112

Note: all the samples were reduced. [a] Determined by ICP-AAS. [b] Diameter of the loading Pt NPs measured by static CO chemisorption, conducted at 303 K. [c] Surface area determined from N_2 adsorption and desorption isotherms. [d] Evaluated for approximately 100 particles from TEM images. [e] Determined by MDI Jade 5 software.

Table 2. Compositional and reduction properties of CeO_2, 0.6Pt/CeO_2, 0.9Pt/CeO_2, 0.6Pt/CeO_2-A and 0.9Pt/CeO_2-A catalysts.

Samples	$Pt^0/(Pt^0 + Pt^{2+})$ (%)	N1/(N1 + N2 + N3) (%)	$Ce^{3+}/(Ce^{3+} + Ce^{4+})$ (%)	$O_{sur}/(O_{latt} + O_{sur})$ (%)	I_D/I_{F2g}	Peak Position (°C)	H_2 Consumption (μmol g^{-1})
CeO_2	/	/	32.06	35.34	1.584	511	231
0.6Pt/CeO_2	68.74	/	35.82	35.97	1.649	98, 337, 508	96, 195, 142
0.9Pt/CeO_2	71.29	/	36.34	38.84	1.825	95, 336, 505	113, 187, 165
0.6Pt/CeO_2-A	69.65	29.28	36.26	36.14	1.662	91, 322, 504	126, 111, 112
0.9Pt/CeO_2-A	71.21	38.39	37.18	37.55	1.910	92, 324, 505	132, 108, 101

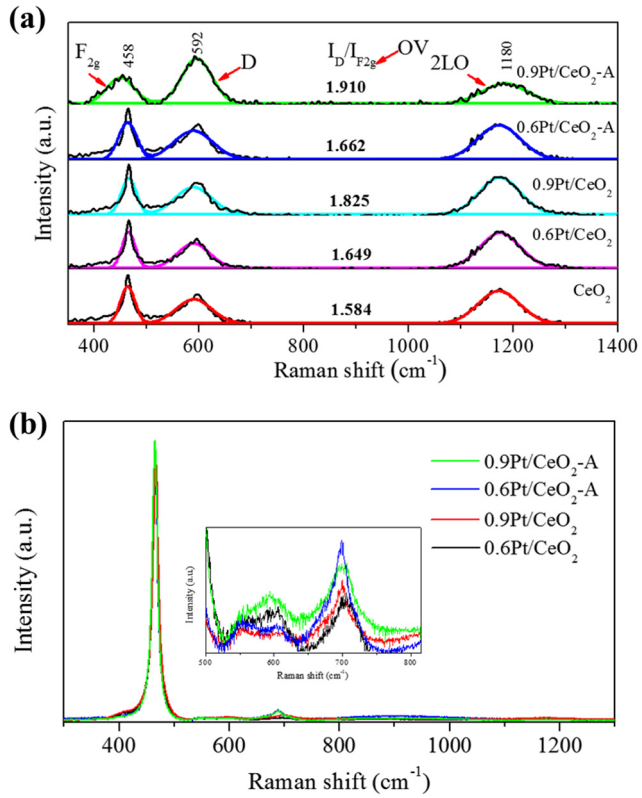

Figure 4. The Raman spectra of (**a**) UV and (**b**) Visible for CeO_2, 0.6Pt/CeO_2, 0.9Pt/CeO_2, 0.6Pt/CeO_2-A and 0.9Pt/CeO_2-A catalysts.

The reducibility of CeO_2 and Pt/CeO_2 samples has been systematically investigated as reported in H_2-TPR, with the findings illustrated in Figure 5. The H_2 consumption data are summarized in Table 2. The pure CeO_2 exhibits a single broad peak in the temperature range below 600 °C, indicative of the reduction of surface and subsurface oxygen species [9]. Upon the introduction of Pt, the reduction profiles display significant alterations, with the emergence of two distinct peaks. The initial peak, observed at approximately 90 °C, can be ascribed to the reduction of PtO_x. It is crucial to highlight that the H_2 consumption for this peak is significantly greater than that recorded when Pt remains entirely tetravalent, with values of approximately 61 μmol g^{-1} for 0.6 wt.% Pt loading and 92 μmol g^{-1} for 0.9 wt.% Pt loading. This increased H_2 consumption strongly suggests a spillover effect of oxygen species on the surface and subsurface regions adjacent to the Pt, driven by the SMSI between Pt and the CeO_2 support. Such findings underscore the transformative impact of platinum on enhancing the reducibility of CeO_2. The second peak observed at 300–350 °C clearly demonstrates the reduction of surface oxygen species, profoundly influenced by the incorporation of Pt. This observation underscores the considerable presence and size of unstable surface oxygen vacancies, which are critical for understanding the material's reactivity and stability.

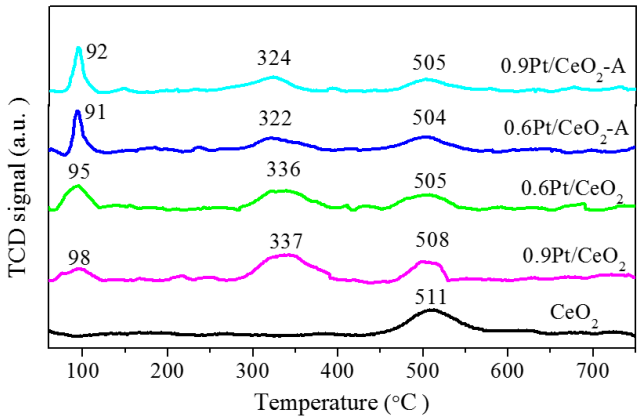

Figure 5. H_2-TPR profiles of CeO_2, 0.6Pt/CeO_2, 0.9Pt/CeO_2, 0.6Pt/CeO_2-A and 0.9Pt/CeO_2-A catalysts.

2.2. Catalytic Activity Evaluation

The catalytic performance of Pt/CeO_2 and CeO_2 samples was assessed through toluene catalytic degradation tests, as illustrated in Figure 6a. Notably, the 0.9Pt/CeO_2-A sample demonstrated a remarkable reduction in the temperature required for 50% and 90% conversion of toluene, occurring at 136 °C and 149 °C (at a weight hourly space velocity of 48,000 mL g^{-1} h^{-1}), respectively. These values are significantly lower compared to the CeO_2 sample, as detailed in Table 3, which indicates a decrease of 135 °C and 147 °C for T_{50} and T_{90}, respectively. Furthermore, samples that underwent pretreatment with anilines (depicted as hollow triangles and hollow circles) exhibited enhanced catalytic activity compared to their untreated counterparts (illustrated as triangles and circles), even when Pt loading remained consistent, highlighting the advantageous impacts of such pretreatment. This enhancement in catalytic activity can be linked to the enhanced SMSI observed in these samples. Notably, each catalyst maintained a high CO_2 selectivity (≥95%), demonstrating consistent effectiveness across all toluene catalytic oxidation tests.

 https://doi.org/10.53941/ges.2025.100007

Previous studies have demonstrated that in a Pt/CeO_2 system, both the Pt nanoparticles and the oxygen vacancies present on the catalyst surface serve as active sites that significantly influence the reaction rate [11]. The turnover frequencies for oxygen vacancies (TOF_{OV}) and for PT (TOF_{Pt}) are calculated separately and presented in Table 3. The observed sequence of catalytic activity aligns with the trends observed in both TOF_{OV} and TOF_{Pt}, corroborating findings from earlier research.

Additionally, the Arrhenius plots depicting the conversion of toluene are presented in Figure 6b. The activation energies (E_a) for toluene conversion were determined from the slope of the linear regression of the Arrhenius scatter plots and are compiled in Table 3. The calculated E_a values for the different samples exhibited the following order: $0.9Pt/CeO_2$-A < $0.9Pt/CeO_2$ < $0.6Pt/CeO_2$-A < $0.6Pt/CeO_2$ < CeO_2. This clear sequence suggests an inverse relationship between catalytic activity and E_a values, indicating that as the activation energy increases, the catalytic efficiency diminishes. Such findings underscore that toluene combustion is significantly enhanced in the presence of the Pt/CeO_2-A catalysts, highlighting their superior catalytic performance.

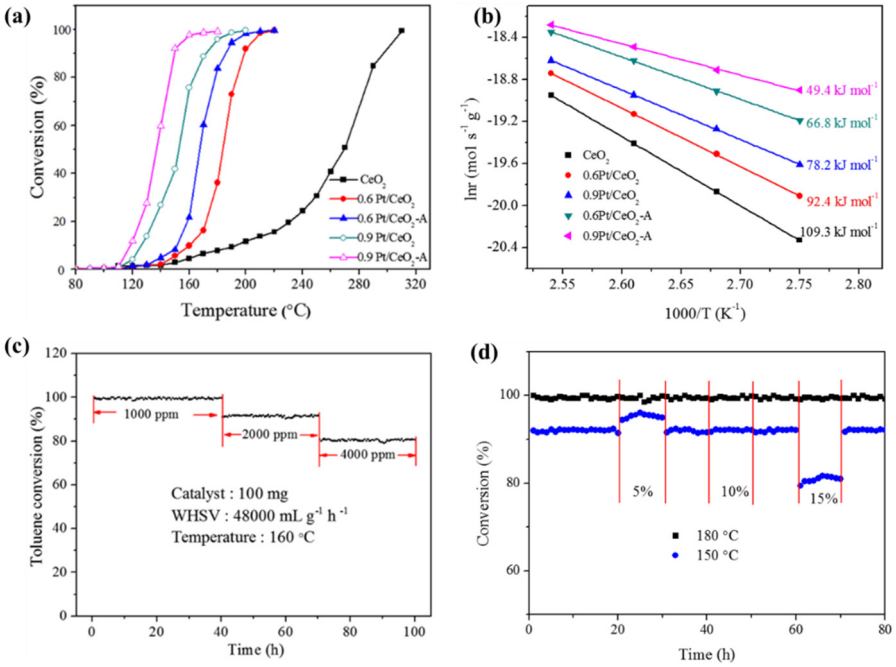

Figure 6. Catalytic performances over CeO_2, $0.6Pt/CeO_2$, $0.9Pt/CeO_2$, $0.6Pt/CeO_2$-A and $0.9Pt/CeO_2$-A catalysts. (**a**)The light-off performance (**b**)Arrhenius fitting curves (**c**) stability and (**d**) H_2O resistance test for toluene catalytic oxidation over various Pt/CeO_2 catalysts.

Table 3. Catalytic performances of CeO_2, $0.6Pt/CeO_2$, $0.9Pt/CeO_2$, $0.6Pt/CeO_2$-A and $0.9Pt/CeO_2$-A catalysts.

Samples	Catalytic Activity		TOF_{OV} (10^{-3} s^{-1})	TOF_{Pt} (10^{-4} s^{-1})	E_a (kJ mol^{-1})
	T_{50} (°C)	T_{90} (°C)			
CeO_2	271	296	0.8	/	109.3
$0.6Pt/CeO_2$	183	200	5.54	4.55	92.4
$0.9Pt/CeO_2$	152	173	6.98	5.25	78.2
$0.6Pt/CeO_2$-A	167	185	12.67	17.26	66.8
$0.9Pt/CeO_2$-A	136	149	13.62	34.92	49.4

2.3. Durability and Water Resistance Test

The durability of toluene oxidation over the most effective catalyst, $0.9Pt/CeO_2$-A, was assessed at a reaction temperature of 160 °C, as illustrated in Figure 6c. Notably, the $0.9Pt/CeO_2$-A catalyst exhibited the unique characteristic of exclusively generating CO_2 as a by-product, with no carbon-containing species detected in the tail gas during toluene catalytic oxidation. The results indicate that the catalytic activity for toluene remains largely stable throughout a continuous 40-h evaluation period. However, upon increasing the toluene concentration to 2000 ppm, a marked decrease in conversion was observed, dropping to 91%. Furthermore, when the toluene concentration was raised again to 4000 ppm, the conversion further declined to 80%. Despite these fluctuations, the toluene conversion remained relatively stable across varying concentrations, underscoring the exceptional durability of the $0.9Pt/CeO_2$-A catalyst.

The 0.9Pt/CeO_2-A catalyst demonstrates exceptional catalytic activity in dry gas conditions. However, as water is a significant byproduct of toluene catalytic combustion, it is known to adversely affect catalytic performance. Therefore, the catalytic behavior of the 0.9Pt/CeO_2-A catalyst was investigated under vapor conditions with varying water concentrations (5 vol%, 10 vol%, and 15 vol%) at temperatures of 150 °C and 180 °C, as depicted in Figure 6d. Notably, upon the introduction of 5% water vapor at 150 °C, the toluene conversion notably increased from 92% to 95%. When the water vapor concentration was elevated to 10%, the toluene conversion rate remained relatively stable over time. However, at a water vapor content of 15%, a slight decrease in toluene conversion was observed, dropping from 92% to approximately 90%. When the reaction was conducted at 180 °C, no significant deactivation of the 0.9Pt/CeO_2-A catalyst was observed. This phenomenon may be attributed to the catalyst's enhanced activity at elevated temperatures, which potentially generates additional active sites, thus maintaining its efficacy.

The deactivation of catalytic activity in the presence of water vapor is primarily attributed to the competitive adsorption of water and toluene [32]. However, an optimal concentration of surface hydroxyl groups may enhance the catalytic reaction involving toluene. At lower concentrations of water vapor, the competition between H_2O and toluene for adsorption sites exerts minimal influence on the reaction, thereby facilitating catalytic activity. In contrast, as the concentration of water vapor increases, it begins to dominate the adsorption process, thereby obstructing the catalytic reaction. Notably, when the reaction is conducted at 180 °C, no significant deactivation of the 0.9Pt/CeO_2-A catalyst is observed. This may be attributable to the catalyst's heightened activity at elevated temperatures, which can provide additional active sites. Upon the introduction of water vapor following each stop, the catalytic activity was swiftly restored to its original levels, with the toluene conversion reverting to baseline values. This observation indicates that, under water vapor conditions, all catalysts except for 0.9Pt/CeO_2-A exhibit varying degrees of deactivation, particularly under elevated water vapor concentrations. In contrast, catalysts modified with aniline demonstrated a lesser degree of reduction in activity. These findings suggest that aniline-pretreated catalysts possess enhanced tolerance to water vapor, thereby maintaining commendable catalytic activity within a specific temperature range.

3. Experimental Section

3.1. Catalysts Preparation

3.1.1. Preparation of CeO_2 with Well-Defined Facets

All the reagents used were of analytical purity without further purification. The CeO_2 support with well-defined facets was prepared via hydrothermal methods as published in our previous work [11]. Please refer to the Supplementary Materials for a detailed explanation of the synthesis procedure.

3.1.2. Preparation of xPt/CeO_2-A and xPt/CeO_2

Initially, 1 g of the above-prepared CeO_2 was dissolved in 20 mL of a mixed solution comprising equal parts water and ethanol (molar ratio of 1:1). Subsequently, 20 μL of aniline was introduced to the aforementioned solution while maintaining vigorous agitation. The mixture was stirred for 2 h, after which an appropriate quantity of chloroplatinic acid hexahydrate (H_2PtCl_6) was added to achieve Pt loadings of 0.6 wt.% and 0.9 wt.%. This solution was then subjected to stirring for an additional 12 h. Following this, the mixture was dried at 80 °C overnight. The resulting brown-black powder was subsequently calcined at 500 °C for 3 h in a nitrogen atmosphere, followed by a treatment at 400 °C for 4 h in dry air. The catalysts obtained through this process were designated as xPt/CeO_2-A, where x represents the specific Pt loading content. The synthesis of the xPt/CeO_2 catalysts followed a similar protocol as that of xPt/CeO_2-A, with the notable exception of omitting the addition of aniline. The catalysts produced in this manner were referred to as xPt/CeO_2, with x again denoting the Pt loading content.

3.2. Catalysts Characterizations

The physicochemical properties of these samples were extensively investigated employing a diverse array of advanced characterization techniques. These techniques include X-ray diffraction (XRD), Brunauer-Emmett-Teller (BET) surface area analysis, scanning electron microscopy (SEM), transmission electron microscopy (TEM), atomic absorption spectroscopy (AAS), X-ray photoelectron spectroscopy (XPS), H_2-TPR, and Raman spectroscopy. A comprehensive overview of the characterization methodologies and the subsequent catalytic performance evaluations can be found in the Supplementary Materials.

3.3. Catalytic Activity Evaluation

Our previous work provides a comprehensive overview of the evaluations conducted on catalytic activity, catalyst durability, and H_2O resistance tests [32]. The detailed procedures are presented in the Supplementary Materials.

4. Conclusions

In summary, we have successfully developed the Pt/CeO_2 catalyst with and without aniline pretreatment.

 https://doi.org/10.53941/ges.2025.100007

Our investigations employing various techniques, including TEM, XPS, and Raman spectroscopy, reveal compelling results. Notably, aniline modification significantly enhances the Strong Metal-Support Interaction, leading to improved dispersion of Pt particles and the formation of oxygen vacancies. Among all examined samples, the 0.9Pt/CeO_2-A catalyst stands out, showcasing the highest catalytic activity and durability. This exceptional performance is attributed to the optimal dispersion of Pt species, alongside an increase in both Pt^0 and Ce^{3+} ions, as well as abundant surface oxygen vacancies. We strongly believe that the strategies presented herein could serve as a transformative approach to boost the activity and stability of other CeO_2-supported nanocatalysts.

Supplementary Materials

The following supporting information can be downloaded at: https://media.sciltp.com/articles/others/2507311419588667/GES-1260-SI.pdf.

Author Contributions

D.Y. (Dengfeng Yan): conceptualization, funding acquisition, investigation, writing-original draft preparation and writing-review and editing; Z.F.: formal analysis, investigation, and writing-original draft preparation; X.L., Y.W. and S.G.: investigation and writing-review and editing; D.Y. (Daiqi Ye): supervision and funding acquisition. All authors have read and agreed to the published version of the manuscript.

Funding

This research described above was financially supported by the National Natural Science Foundation of China (No. 82204009), the Medical Scientific Research Foundation of Guangdong (No. A2022238), the Science and Technology Project of Guangzhou City, China (No. 2023A04J2472).

Institutional Review Board Statement

Not applicable.

Informed Consent Statement

Not applicable.

Conflicts of Interest

The authors declare no conflict of interest.

References

1. Mu, J.; Zhang, Y.; Xia, Z.; et al. Two-year online measurements of volatile organic compounds (VOCs) at four sites in a Chinese city: Significant impact of petrochemical industry. *Sci. Total Environ.* **2023**, *858*, 159951.
2. Liu, Y.; Yin, S.; Zhang, S.; et al. Drivers and impacts of decreasing concentrations of atmospheric volatile organic compounds (VOCs) in Beijing during 2016–2020. *Sci. Total Environ.* **2024**, *906*, 167847.
3. Zhou, X.; Zhou, X.; Wang, C.; et al. Environmental and human health impacts of volatile organic compounds: A perspective review. *Chemosphere* **2023**, *313*, 137489.
4. Pye, H.O.T.; Appel, K.W.; Seltzer, K.M.; et al. Human-Health Impacts of Controlling Secondary Air Pollution Precursors. *Environ. Sci. Technol. Lett.* **2022**, *9*, 96–101.
5. Wang, H.; Sun, S.; Nie, L.; et al. A review of whole-process control of industrial volatile organic compounds in China. *J. Environ. Sci.* **2023**, *123*, 127–139.
6. Zhang, H.; Wang, Z.; Wei, L.; et al. Recent progress on VOC pollution control via the catalytic method. *Chin. J. Catal.* **2024**, *61*, 71–96.
7. Kim, H.-S.; Kim, H.-J.; Kim, J.-H.; et al. Noble-Metal-Based Catalytic Oxidation Technology Trends for Volatile Organic Compound (VOC) Removal. *Catalysts* **2022**, *12*, 63.
8. Lou, B.; Shakoor, N.; Adeel, M.; et al. Catalytic oxidation of volatile organic compounds by non-noble metal catalyst: Current advancement and future prospectives. *J. Clean. Prod.* **2022**, *363*, 132523.
9. Yan, D.; Li, X.; Zhong, J.; et al. Tuning the Metal–Support Interaction by Modulating CeO_2 Oxygen Vacancies to Enhance the Toluene Oxidation Activity of Pt/CeO_2 Catalysts. *Inorg. Chem.* **2024**, *63*, 11393–11405.
10. Peng, R.; Wen, S.; Zhang, H.; et al. Catalytic Oxidation of Toluene over Pt/CeO_2 Catalysts: A Double-Edged Sword Effect of Strong Metal–Support Interaction. *Langmuir* **2024**, *40*, 13984–13994.
11. Peng, R.; Sun, X.; Li, S.; et al. Shape effect of Pt/CeO_2 catalysts on the catalytic oxidation of toluene. *Chem. Eng. J.* **2016**, *306*, 1234–1246.
12. van Deelen, T.W.; Hernández Mejía, C.; de Jong, K.P. Control of metal-support interactions in heterogeneous catalysts to enhance activity and selectivity. *Nat. Catal.* **2019**, *2*, 955–970.
13. Li, Y.; Zhang, Y.; Qian, K.; et al. Metal–Support Interactions in Metal/Oxide Catalysts and Oxide–Metal Interactions in Oxide/Metal Inverse Catalysts. *ACS Catal.* **2022**, *12*, 1268–1287.
14. Luo, Z.; Zhao, G.; Pan, H.; et al. Strong Metal–Support Interaction in Heterogeneous Catalysts. *Adv. Energy Mater.* **2022**, *12*, 2201395.
15. Zhang, J.; Qin, X.; Chu, X.; et al. Tuning Metal–Support Interaction of Pt-CeO_2 Catalysts for Enhanced Oxidation Reactivity. *Environ. Sci. Technol.* **2021**, *55*, 16687–16698.
16. Eliasson, H.; Niu, Y.; Palmer, R.E.; et al. Support-facet-dependent morphology of small Pt particles on ceria. *Nanoscale* **2023**, *15*, 19091–19098.
17. Castro-Latorre, P.; Neyman, K.M.; Bruix, A. Systematic Characterization of Electronic Metal–Support Interactions in Ceria-Supported Pt Particles. *J. Phys. Chem. C* **2023**, *127*, 17700–17710.
18. Ge, S.; Fan, W.; Tang, X.; et al. Revealing the Size Effect of Ceria Nanocube-Supported Platinum Nanoparticles in Complete Propane Oxidation. *ACS Catal.* **2024**, *14*, 2532–2544.

19. Yang, B.; Chen, X.; Guo, L.; et al. Catalyst architecture for metal–support interactions and its effects on heterogeneous reactions. *J. Mater. Chem. A* **2024**, *12*, 19861–19884.
20. Wang, T.; Hu, J.; Ouyang, R.; et al. Nature of metal-support interaction for metal catalysts on oxide supports. *Science* **2024**, *386*, 915–920.
21. Pu, T.; Zhang, W.; Zhu, M. Engineering Heterogeneous Catalysis with Strong Metal–Support Interactions: Characterization, Theory and Manipulation. *Angew. Chem. Int. Ed.* **2023**, *62*, e202212278.
22. Ye, S.; Luo, F.; Zhang, Q.; et al. Highly stable single Pt atomic sites anchored on aniline-stacked graphene for hydrogen evolution reaction. *Energy Environ. Sci.* **2019**, *12*, 1000–1007.
23. Zhan, W.; He, Q.; Liu, X.; et al. A Sacrificial Coating Strategy Toward Enhancement of Metal–Support Interaction for Ultrastable Au Nanocatalysts. *J. Am. Chem. Soc.* **2016**, *138*, 16130–16139.
24. Sun, X.-C.; Yuan, K.; Hua, W.-D.; et al. Weakening the Metal–Support Interactions of M/CeO_2 (M = Co, Fe, Ni) Using a NH_3-Treated CeO_2 Support for an Enhanced Water–Gas Shift Reaction. *ACS Catal.* **2022**, *12*, 11942–11954.
25. Matsubu, J.C.; Zhang, S.; DeRita, L.; et al. Adsorbate-mediated strong metal–support interactions in oxide-supported Rh catalysts. *Nat. Chem.* **2016**, *9*, 120–127.
26. Paladugu, S.; Metz, P.C.; Luo, S.; et al. In Situ Neutron Scattering Studies on the Oxidation and Reduction of CeO_2 and Pt–CeO_2 Nanorods. *J. Phys. Chem. C* **2023**, *127*, 3689–3697.
27. Huang, H.; Dai, Q.; Wang, X. Morphology effect of Ru/CeO_2 catalysts for the catalytic combustion of chlorobenzene. *Appl. Catal. B Environ.* **2014**, *158*, 96–105.
28. Yang, Q.; Li, L.; Wang, X.; et al. Tunable metal-support interaction of Pt/CeO_2 catalyst via surfactant-assisted strategy: Insight into the total oxidation of CO and toluene. *J. Hazard. Mater.* **2022**, *424*, 127601.
29. Chen, P.; Khetan, A.; Yang, F.; et al. Experimental and Theoretical Understanding of Nitrogen-Doping-Induced Strong Metal–Support Interactions in Pd/TiO_2 Catalysts for Nitrobenzene Hydrogenation. *ACS Catal.* **2017**, *7*, 1197–1206.
30. Chu, Y. Y.; Cao, J. ; Daia, Z.; et al. A novel Pt/CeO_2 catalyst coated with nitrogen-doped carbon with excellent performance for DMFCs. *J. Mater. Chem. A* **2014**, *2*, 4038–4044.
31. Bi, W.; Hu, Y.; Jiang, H.; et al. In-situ synthesized surface N-doped Pt/TiO_2 via flame spray pyrolysis with enhanced thermal stability for CO catalytic oxidation. *Appl. Surf. Sci.* **2019**, *481*, 360–368.
32. Yan, D.; Li, T.; Liu, P.; et al. In-situ atmosphere thermal pyrolysis of spindle-like Ce(OH)CO_3 to fabricate Pt/CeO_2 catalysts: Enhancing Pt–O–Ce bond intensity and boosting toluene degradation. *Chemosphere* **2021**, *279*, 130658.